Research Article

Highly porous, honeycomb like Ag–ZnO nanomaterials for enhanced photocatalytic and photoluminescence studies: green synthesis using *Azadirachta indica* gum

K. R. Basavalingiah[1,2] · S. Harishkumar[3,4] · Udayabhanu[3] · G. Nagaraju[3] · Dinesh Rangappa[5] · Chikkahanumantharayappa[1]

Abstract

The preparation of zinc oxide and silver doped zinc oxide nanoparticles using zinc nitrates and silver nitrates as oxidizers and *Azadirachta indica* gum as a fuel via solution combustion method at 500 °C. The synthesized nanoparticles were characterized by XRD, FTIR, UV-DRS, SEM and TEM studies; these materials were tested for photoluminescence and photocatalytic activity studies. The PXRD data indicated that the synthesized nanoparticles confirmed as hexagonal phase with average crystallite size of 13.33 and 13.34 nm for ZnO and Ag–ZnO respectively. The SEM data revealed that, the material obtained is highly porous and honeycomb like structure. In the photocatalytic degradation of methylene blue, Ag–ZnO nanoparticles have shown the good photocatalytic activity than undoped ZnO nanoparticles. This is due to the presence of Ag on the surface of ZnO catalyst makes the catalyst more sensitive to light and reduce the electron hole recombination. Furthermore, we have also examined the photoluminescence studies for the synthesized materials and it has given the green emission by excitation at 380 nm. In this study, the green synthesis method will produces large quantity of nanomaterials with less time and low cost.

Keywords Green synthesis · *Azadirachta indica* · Honeycomb · Silver zinc oxide · Photocatalytic · Photoluminescence

1 Introduction

Paper, dyeing, plastic and textile industries use colour for staining their products and consuming large amount of water to clean, it can lead formation of waste water with dye and it can harmful to the nature [1–4]. Currently, 100,000 various types of dyes produced with an annual production rate of 7×10^5. Among them, textile industries consume dye about 36,000 ton/year, 10–20% of which release dye content waste water in to the environment can lead to pollute the marine life. Hence it is a very important task to reduce releasing of dye and organic pollutant in to the aquatic life.

Presently, the photocatalysis has attracted special attention as an economic and environmentally safe option for solving energy and pollution problems [5].

From the literature survey, the synthesized nanoparticles (Nps) by greener approach methods are useful for pharmaceutical applications and waste water treatment [6]. The advantages of using plant extracts in Ag NPs fabrication is non-hazardous simplicity in scaling up synthesis [7]. In the current work, ZnO nanoparticles are prepared by a novel, simple, efficient, environment friendly and green

✉ Chikkahanumantharayappa, chrayappa@gmail.com | [1]Department of Physics, Vivekananda Degree College, Bangalore, Karnataka 560055, India. [2]Department of Science, Government Polytechnic, Tumkur, Karnataka 572103, India. [3]Energy Materials Research Laboratory, Department of Chemistry, Siddaganga Institute of Technology, Tumkur, Karnataka 572103, India. [4]Department of Pharmaceutical Chemistry, Post-Graduate Centre, Kuvempu University, Kadur, Karnataka 572103, India. [5]Department of Nanoscience and Nanotechnology, VTU Muddenahalli, Chikkaballapur, Karnataka 562103, India.

SN Applied Sciences (2019) 1:935 | https://doi.org/10.1007/s42452-019-0863-z

Received: 3 March 2019 / Revised: 21 June 2019 / Accepted: 28 June 2019 / Published online: 29 July 2019

route using *Azadirachta indicagum* extract, which plays as a fuel. It is also reported that using leaf extract, it is possible to control the shape and size of the particles. Being biotemplates, it also hinders agglomeration of nanoparticles [8].

ZnO is an important and distinctive inorganic substance, because of its distinctive characteristics and novel applications in various fields of science and technology [9]. ZnO has capacity to exhibit piezoelectric, pyroelectric, optoelectronic, catalysis and semiconducting properties [10]. Due to this, ZnO is a multifunctional compound which is used in the field of light emitting diodes, biosensors, diluted and ferromagnetic materials for spintronics solar cells, photocatalysis, transistors and also acts as antioxidants and antibacterial agent [11–13]. ZnO is the most prominent n-type wide band gap metal oxide semiconductor (~ 3.37 eV) with high excitation binding energy (60 m eV) [14–17]. Various methods were discovered for synthesize of ZnO Nps such as hydrothermal, direct precipitation, sol–gel and solvothermal methods [18–23]. These methods need costliest starting material, lengthy procedures, sophisticated apparatus and more time required. But the neem gum assisted combustion method was constructed as it is an easier, less energy and time consuming method among all the methods. The major advantages of green synthesis was reduce pollution to the globe and useful for synthesis materials easily, eco-friendly and reasonable quantities.

Neem Gum, a distinctive plant gum that originates from the neem tree (Melia Azidirachta, maliaceae) is a complex polysaccharide acid salt. It has been medicinally used in India for many centuries [24]. Neem gum on hydrolysis yields D-galactose, D-glucuronic acid, L-fucose and L-arabinose (Fig. 1). The aldobiuronic acid is the ingredient of neem gum derived from graded hydrolysis is shown to be 4-O-(D-glucopyranosyluronic acid)-D-galactopyranose.

The present work reports the synthesis of ZnO and Ag–ZnO NPs using neem gum as fuel. The prepared NPs were characterized using powder X-ray diffraction (PXRD), Fourier transform infrared analysis (FTIR), UV-diffused reflectant spectrum (UV-DRS), scanning electron microscopy (SEM) and transmission electron microscopy (TEM) of the ZnO NPs.

2 Experimental

2.1 Preparation of ZnO and Ag–ZnO Nps

Preparation of ZnO and Ag–ZnO Nps was employed by combustion method. Zinc nitrate and Silver nitrate were used as precursors and *Azadirachta indica* gum was used as a fuel.

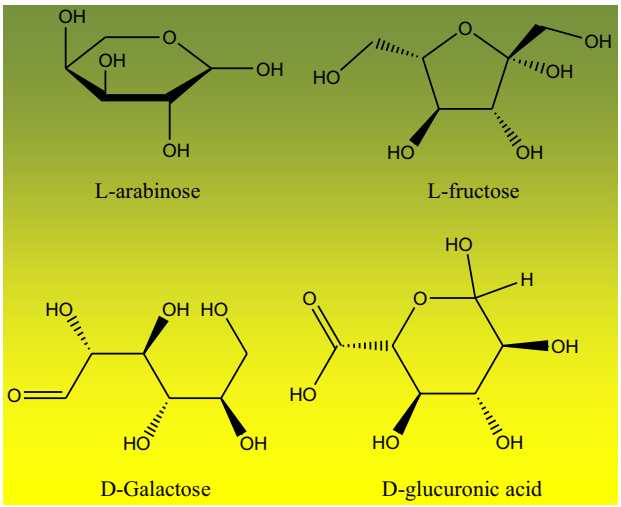

Fig. 1 Major compounds present in neem gum

The stoichiometric ratios of $Zn(NO_3)_2{\cdot}6H_2O$ and $Ag(NO_3)$ were taken in a beaker with varying concentrations *Azadirachta indica* gum (120, 240, 360, 480, 600 mg) with 15 mL of H_2O. The solution is stirred until to become homogeneous. This mixture is taken into a preheated muffle furnace maintained at 500 °C, the smoldering type of the combustion reaction occurs and nanocrystalline ZnO was formed within 5 min. The schematic representation for the synthesis Ag–ZnO was shown in Fig. 2.

2.2 Characterization

XRD data were recorded in Rigaku Smart Lab. FTIR analysis was recorded using Bruker Alpha-p spectrometer. The morphology of the synthesized nanoparticles was observed using SEM (Hitachi-7000 Table top). Shape and size of the nanoparticles were determined by TEM (JEOL 3010). Photoluminescence (PL) studies were recorded using fluorescence spectrophotometer (Agilent technology Cary Eclipse).

2.3 Photocatalytic degradation of dye

Prepared ZnO and Ag doped ZnO nanoparticles were taken for degradation of methylene blue (MB) using 120 W light for source of radiation. 5, 10, 15, and 20 mg of photocatalyst were added to 100 mL of various concentrations of MB solutions (5, 10, 15, and 20 ppm) in a HEBER photo reactor [25]. The solution was continuously mixed by passing air in dark for 30 min to confirm adsorption–desorption equilibrium between MB and photocatalyst before irradiation. Suspension (2 mL) was taken from the solution mixture at intervals of 30 min. The dispersed ZnO/Ag–ZnO photocatalyst was removed using a spin win

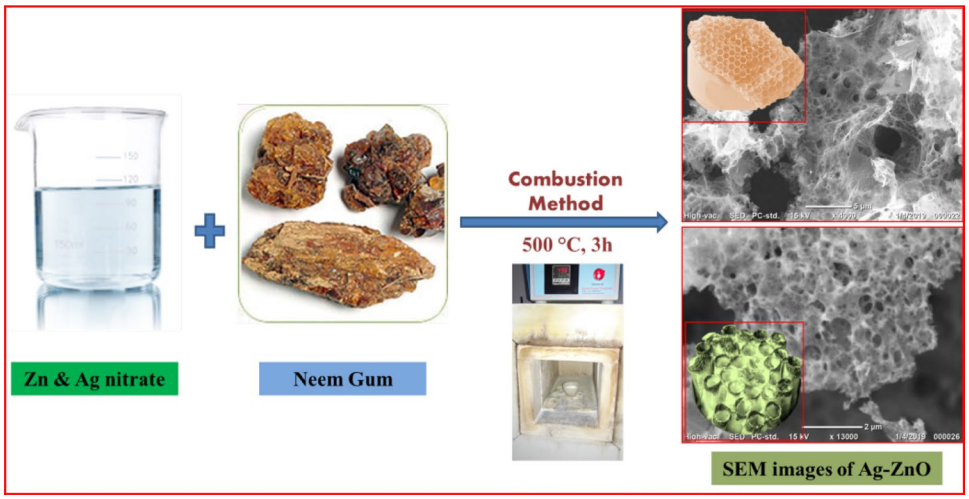

Fig. 2 Graphical representation for the synthesis of ZnO and Ag–ZnO nanomaterials by combustion method

microcentrifuge. The degradation % can be calculated using the formula.

$$\% \text{ of degradation} = \left(C_i - C_f\right)/C_i \times 100 \quad (1)$$

where C_i and C_f are the initial and final concentration of the dye.

3 Results and discussion

3.1 XRD study

The XRD patterns of ZnO and Ag–ZnO Nps are shown in Fig. 3. The pure ZnO (Fig. 1a) displays XRD pattern peaks, that can at 2θ = 31.91°, 34.58°, 36.37° and 47.52° were indexed with the planes (101) (002) (101) and (102) for the resultant particles with Hexagonal phase. The structure of the resultant data is according to the JCPDS card number 3-888. The XRD pattern of Ag–ZnO Nps (Fig. 1b) shows an additional peaks at 38.1° (111) and 44.1° (200) compared to undoped ZnO Nps corresponding to cubic phase silver (JCPDS number 2-109) [26]. The average crystallite size was calculated using Debye–Scherrer equation and it was found to be 13.34 and 13.33 nm for ZnO and Ag–ZnO Nps respectively.

$$D = K\lambda/\beta \cos\theta \quad (2)$$

where, K is constant (0.94), λ is wavelength, β is the full width at half maxima and D is the crystallite size.

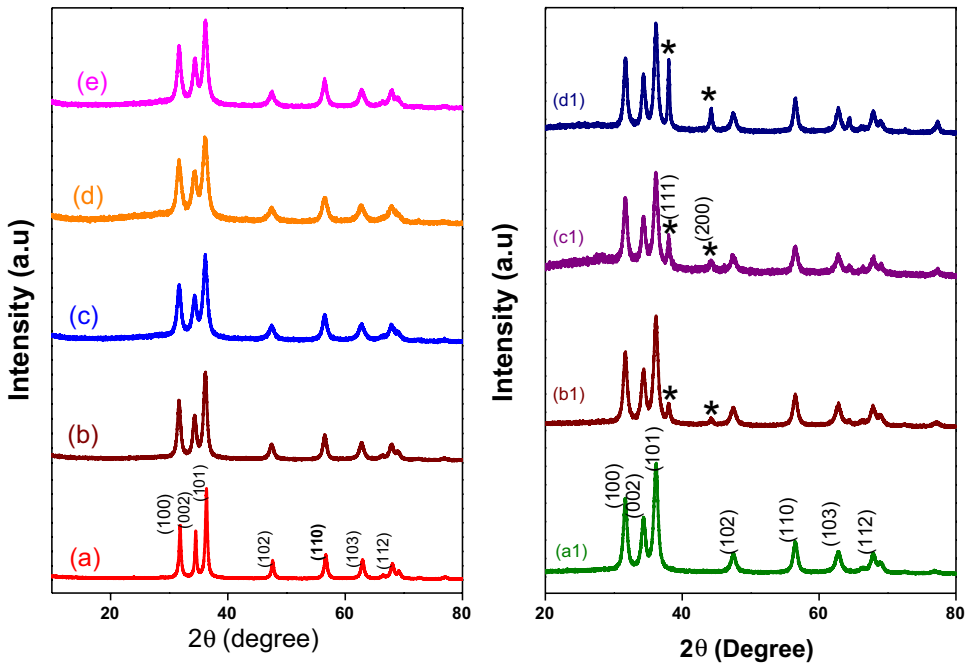

Fig. 3 Powder XRD patterns of the ZnO nanopowders prepared by (a) 120 mg, (b), a1 240 mg, (c) 360 mg, (d) 480 mg, (e) 600 mg of neem gum. (b1) 3% (c1) 5% and (d1) 7% Ag–ZnO synthesized using 240 mg of neem gum

To study the structural changes in the different catalysts were examined with the help of Rietveld refinement studies. To get exact lattice parameters, Rietveld refinement analysis (Fig. 4) was performed by using FULLPROOF software assuming P63mc (186) space group for hexagonal structure. Pseudo-voigt function was utilized to fit the various parameters to the data point. Diamond software was utilized for extracting the possible packing diagram (Fig. 5), from which we cannot see the presence of Ag atoms in a ZnO crystals this might be less concentration of dopant. The refined parameters such as occupancy, atomic functional positions are displayed in Table 1. The fitting parameters (R_p, R_{wp} and χ^2) indicate a good agreement between the refined and observed PXRD patterns for the hexagonal ZnO phase.

As the doping concentration increases there will be an increase of density and decrease of cell volume this is due to the addition of Ag ions in the crystal of ZnO. The χ^2 value is increases from pure ZnO to 7% Ag doped ZnO. This indicates that there is a less fitting with standard graph due to interfering Ag ions in the crystallites of ZnO.

3.2 FTIR study

The FTIR spectra of prepared ZnO and Ag–ZnO nanoparticles were recorded from 350 to 4000 cm^{-1}, represented in Fig. 6. In this, significant vibrational band observed in the range of 400–500 cm^{-1} is corresponds characteristic stretching mode of Zn–O bond. In the IR spectra of Ag–ZnO Nps, intensity of the peak is reduced because of the formation of Ag nanoparticles on the surface of ZnO [27]. A broad peak at 3431 cm^{-1} (stretching) and 1330–1670 cm^{-1} (bending) indicates the presence of adsorbed atmospheric moisture [28, 29].

3.3 UV-DRS studies

DRS studies of the synthesized materials were displayed in Fig. 7a. The spectrum displays strong band in between

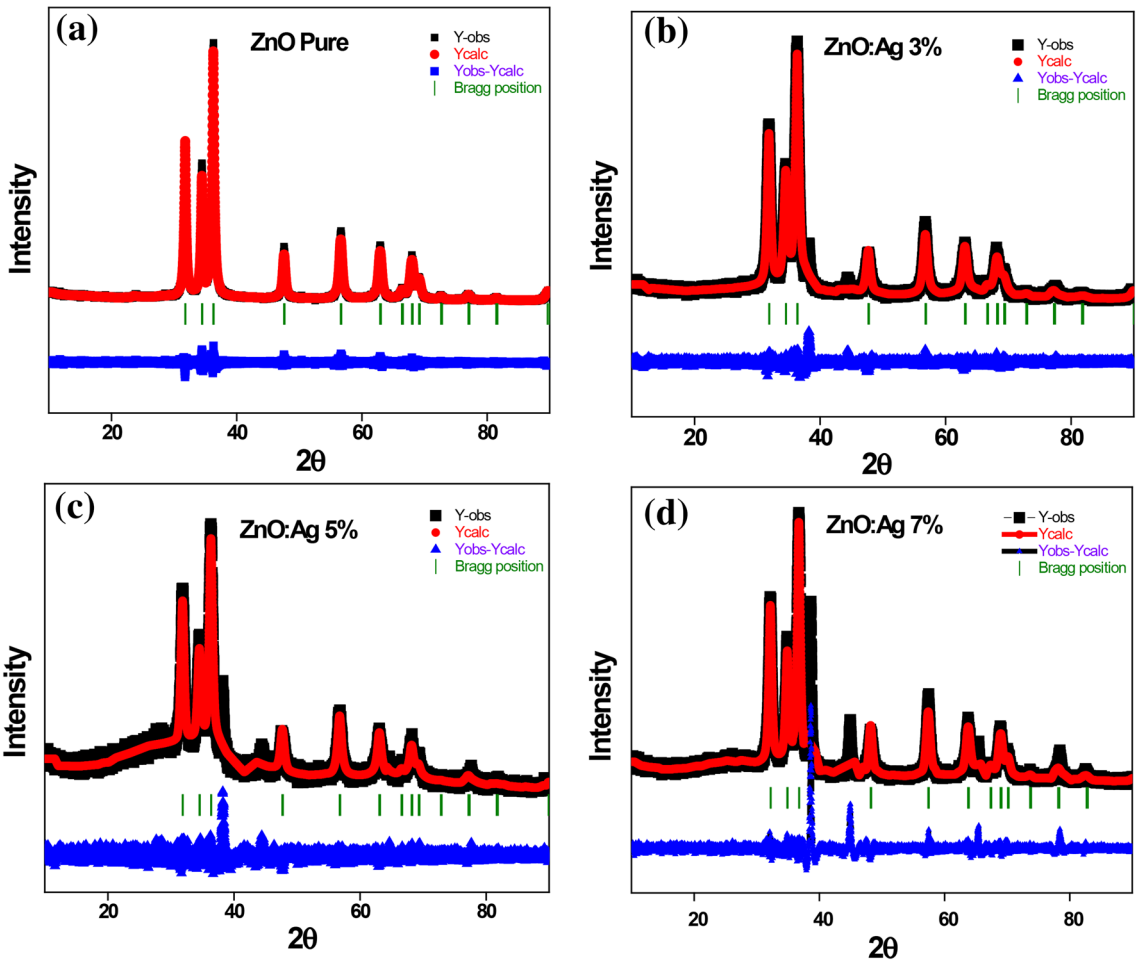

Fig. 4 Rietveld refinement of ZnO and $Ag_{(0-7\%)}$–ZnO PXRD

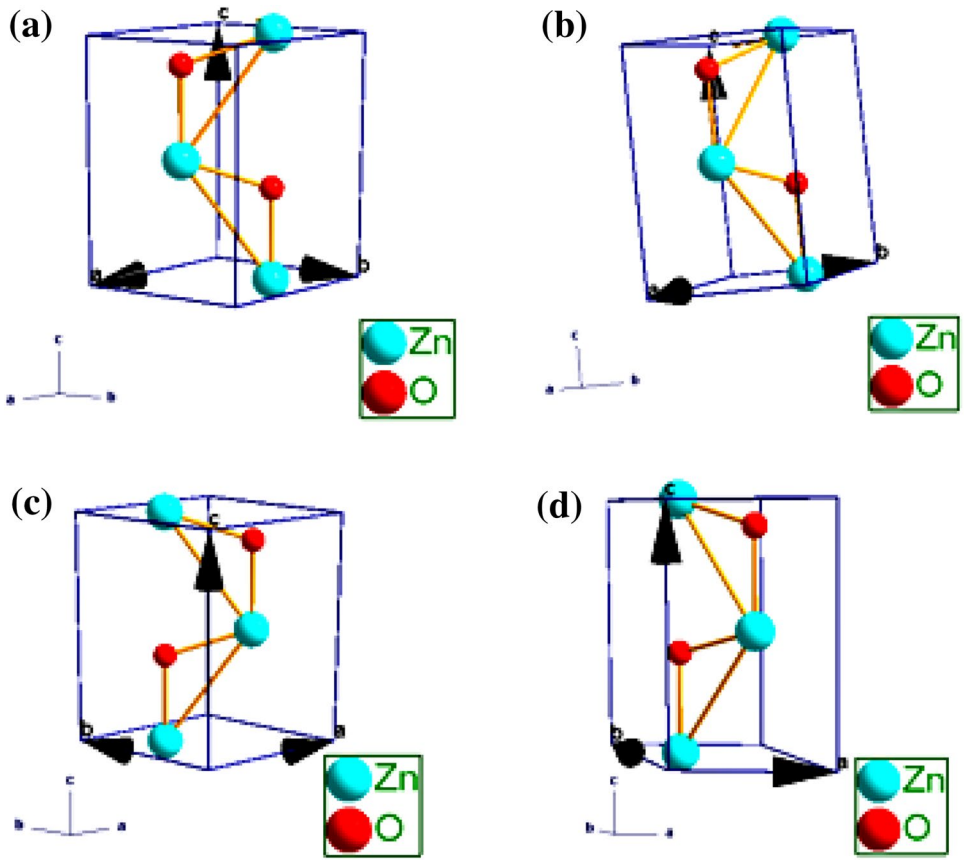

Fig. 5 ZnO packing aiagram **a** Pure **b** Ag doped (3 mol%), **c** 5 mol% and **d** 7 mol%

the wavelength region of 372–390 nm was attributed due to absorption of the host lattice [30]. Figure 7b shows the bandgap of synthesized materials calculated from Kubelka–Munk (KM) function. The obtained energy bandgap (Eg) for synthesized material were tabulated in inset of Fig. 7b.

3.4 SEM studies

SEM images of Ag–ZnO nanomaterials are shown in Fig. 8. From the SEM images it is clearly confirmed that the material synthesized by combustion method is highly porous in nature. The pores were clearly visible in Fig. 8d and the pore diameter is varying from 70 to 500 nm. These pores were created during the synthesis due to the escaping of gases at higher temperatures. The pores were uniformly formed and looks like a honeycomb like structures [31–33].

3.5 TEM studies

Figure 9 shows the TEM images, HR-TEM.images and SAED pattern of synthesized Ag–ZnO porous nanomaterials using *Azardichta indica* gum as a fuel by combustion method. These particles are well dispersed, which acquired the size around 15 nm diameter and these particles are looks like the spherical shape in nature. HR-TEM images give the clear information about the d-spacing values which are different for ZnO and Ag–ZnO. For ZnO the d-spacing value is 0.236 nm, which belongs to the (101) plane and for Ag–ZnO, the d-spacing value is 0.24 nm, which belongs to (111) plane. Presence of Ag on the ZnO material can be easily marked as a dark spots, because the atomic weight of Ag is more than Zn. From the SAED pattern, it is confirmed as a polycrystalline in nature due to the diffracted spots are combined together to form a fringes of circles and these d-spacing values are well matched with the d-spacing values from HR-TEM and also calculated from XRD data.

4 Photocatalytic degradation of ZnO and Ag–ZnO NPs

Under UV irradiation, semiconductor absorbs photon energy with equal to or higher than the bandgap of the semiconductors, it generates electrons and holes on the surface of the photocatalyst. If the charge carriers do not recombine, they can migrate on the surface where free electrons form a reduction of oxygen and form peroxide and superoxide radicals, and the generated

Table 1 Rietveld refined structural parameters for ZnO

Compound	Pure	Ag doped (3 mol%)	Ag doped (5 mol%)	Ag doped (7 mol%)
Crystal system	Hexxagonal	Hexxagonal	Hexxagonal	Hexxagonal
Space group	P63mc (186)	P63mc (186)	P63mc (186)	P63mc (186)
Lattice parameters (A°)				
a = b	3.2493	3.2396	3.2421	3.2087
c	5.2033	5.1891	5.1928	5.1399
α = β	90°	90°	90°	90°
λ	120°	120°	120°	120°
Unit cell volume (A^{o3})	47.575	47.164	47.269	45.829
Density (g/cc^3)	5.6280	5.7320	5.7090	5.9500
Atomic coordinates				
Zn				
x	0.3333	0.3333	0.3333	0.3333
y	0.6667	0.6667	0.6667	0.6667
z	0.0000	0.0000	0.0000	0.0000
O				
x	0.3333	0.3333	0.3333	0.3333
y	0.6667	0.6667	0.6667	0.6667
z	0.3825	0.3794	0.3838	0.3991
Refinement parameters				
R_P	5.72	6.89	7.35	9.74
R_{WP}	7.72	9.98	10.2	16.1
R_{Exp}	7.34	7.59	8.10	8.26
χ^2	1.11	1.73	1.59	3.81
GoF	1.00	1.30	1.30	1.90
R_{Bragg}	1.39	2.26	4.93	8.58
R_F	1.17	2.05	3.50	5.26

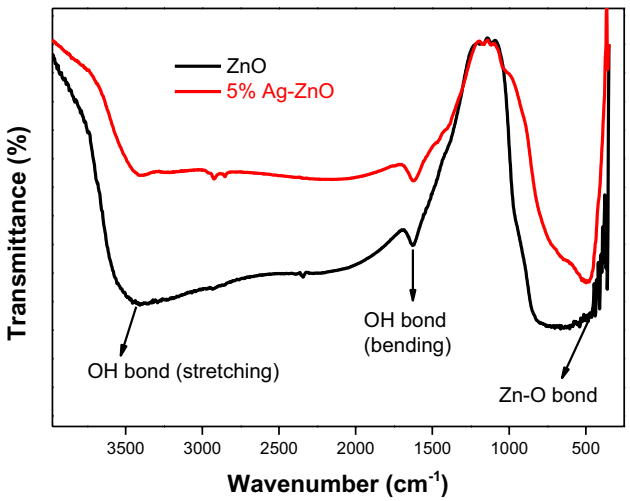

Fig. 6 FTIR spectra of ZnO and Ag–ZnO NPs synthesized by *Azadirachta indica* gum

holes oxidize water and form OH˙. This species is highly reactive and unstable. It ultimately acts on organic compounds and oxidizes carcinogenic dyes to CO_2, water and inorganic acids. The photocatalytic action of the dye is enhanced by various factors of the photocatalyst, namely, particle size, phase composition, shape, crystallinity, size distribution, surface area, surface hydroxyl group density and band gap [34]. Synthetic ZnO NPs were used as photocatalysts to investigate the degradation of methylene blue under UV sources. An aliquot of 2 mL was withdrawn from the UV–Vis reactor for every 30 min, centrifuged and the absorption of the remaining dye was recorded.

Figure 10 displays the photocatalytic degradation activity of bare ZnO and 3, 5, 7% Ag doped ZnO Nps over methylene blue dye. In this 5% Ag doped ZnO Nps exhibits good photocatalytic degradation activity when compared with bare ZnO, 3%, 7% Ag doped ZnO Nps. As the increases of Ag dopant from 3 to 5%, the rate of dye degradation also increases and again increase the Ag dopant from 5 to 7%, the rate of dye degradation was decreased. From this, it is clear that 5% Ag dopant was found to be optimum concentration. When the % of Ag higher than the optimal value, the rate of dye degradation was decreased due to metallic Ag act as recombination centers which is caused by the electrostatic attraction of negatively charged Ag

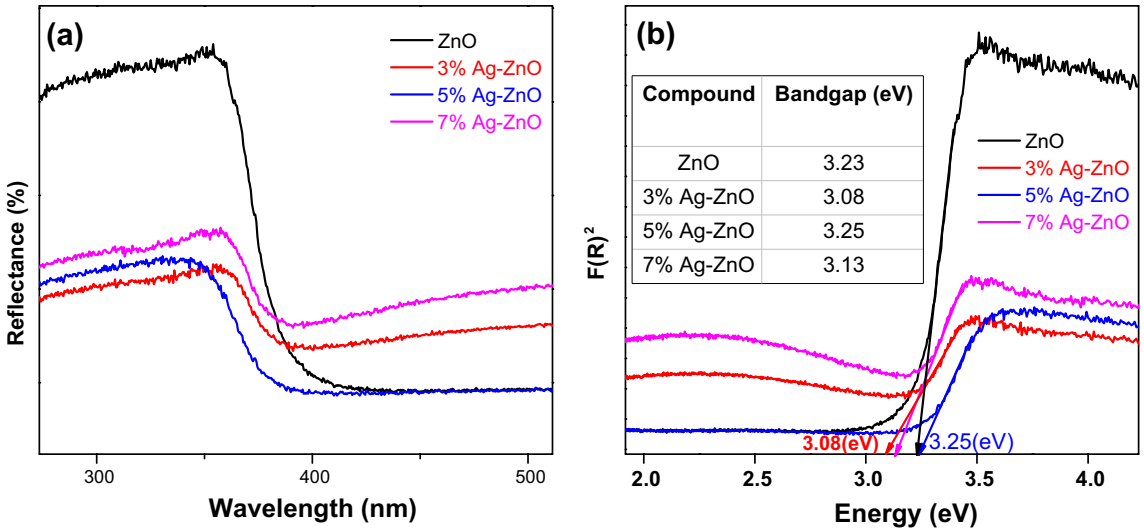

Fig. 7 UV–DRS spectrum of Ag–ZnO NPs synthesized by *Azadirachta indica* gum

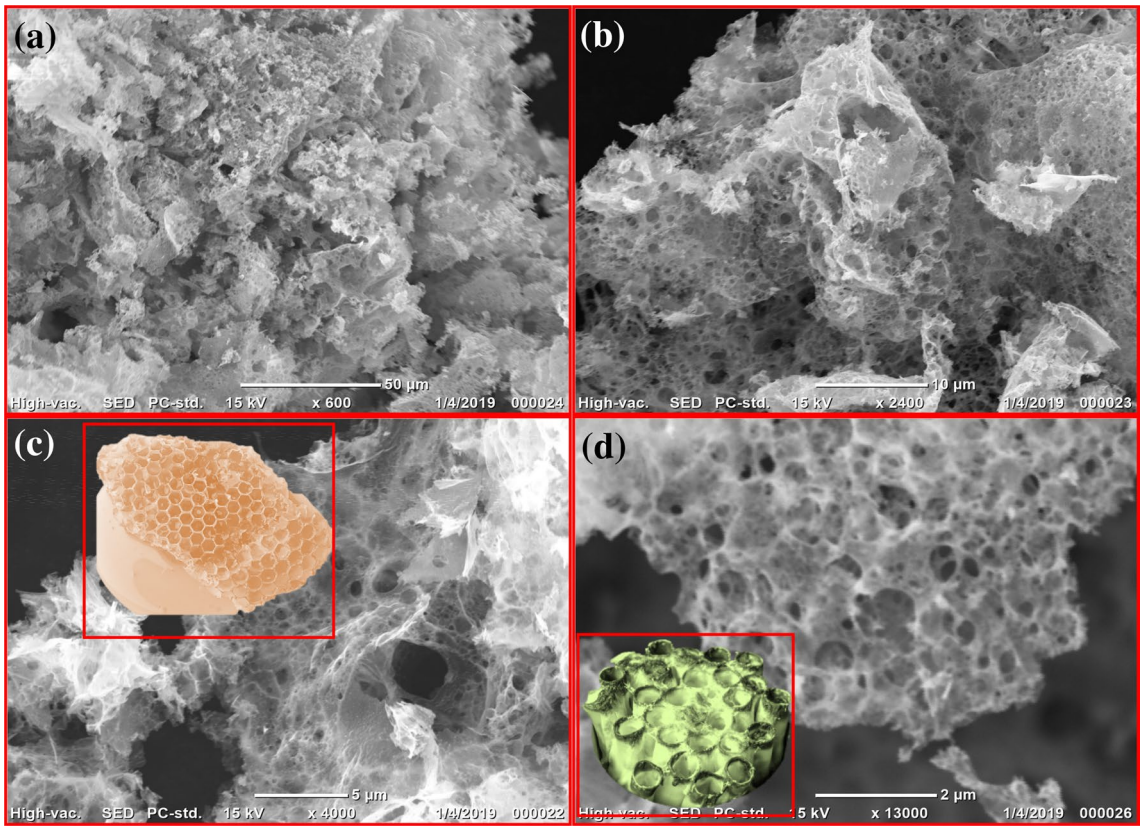

Fig. 8 SEM images of porous Ag–ZnO nanomaterials with different magnification view **a** 50 µm, **b** 10 µm, **c** 5 µm and **d** 2 µm

and positively charged holes. Furthermore excessive Ag reduced the number of photons absorbed by the photocatalyst because of light-filtered effect [35].

4.1 Effect of dye concentration

Photocatalytic activity of ZnO Nps mainly depends on the concentration of the dye. To know the maximum

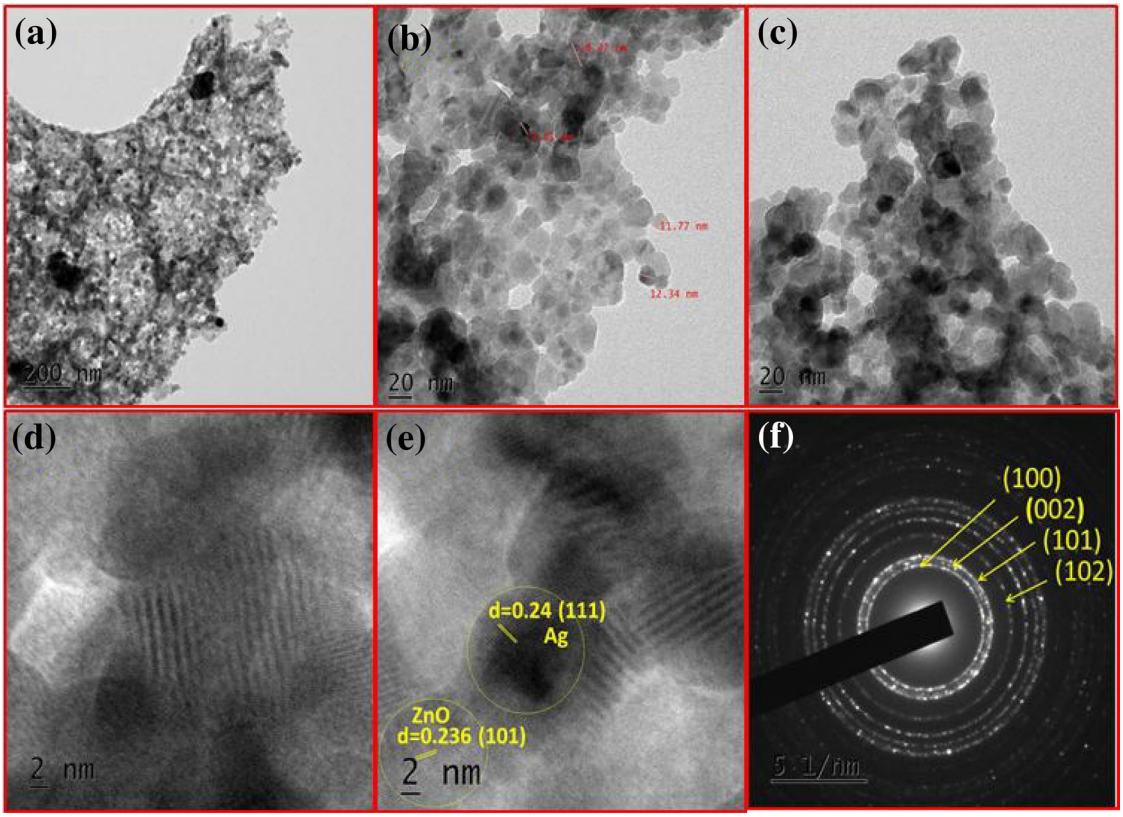

Fig. 9 TEM images (**a**, **b**, **c**), HR-TEM images (**d**, **e**) and SAED pattern (**f**) of Ag–ZnO nanomaterials

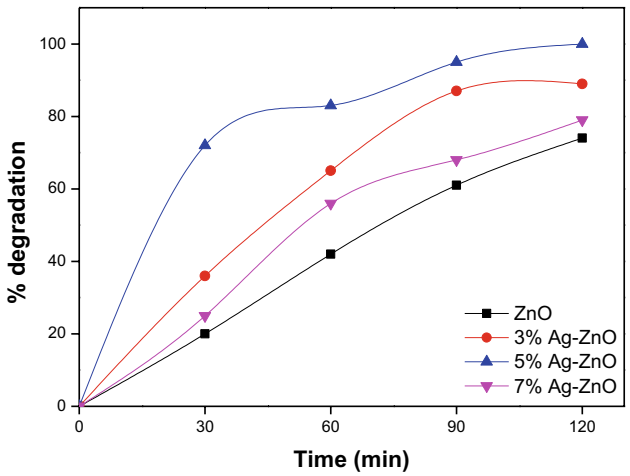

Fig. 10 Photocatalytic degradation of methylene blue with different catalysts

concentration of dye for efficient oxidation, the experiment was carried out by constant catalytic loading (10 mg) and changed the concentration of dye from 5 to 20 ppm with the presence of UV light (Fig. 11). As the dye concentration increases from 5 to 20 ppm, the photocatalytic degradation is reduced from 80 to 20% and 10 ppm is the most effective concentration for dye degradation. Generally, as the concentration of dye increases, rate of degradation was decreases [36].

4.2 Effect of catalyst load

Figure 12 displays the degradation of MB dye with varying catalyst load (5–20 mg) by keeping the dye concentration constant (5 ppm). It is clearly reveals that as the catalyst load increases, the rate of dye degradation increases from 90 to 100%. This is because more active sites are available due to increased catalyst load [37].

4.3 Effect of pH

In order to evaluate the optimal pH for the degradation of MB dye, experiments were conducted at different pH (2 to 12) by maintaining the constant catalyst load (10 mg) and concentration of dye (5 ppm), the data was represented in Fig. 13. It reveals that the degradation of MB was excellent in the basic condition [38, 39] with the highest rate of degradation observed at pH 10. Above this pH the degradation decreases, and can be explained on the basis of zero potential charge (ZPC). For ZnO, ZPC is 9.0 ± 0.3, and if it exceeds this value, the adsorbed OH^- ions form the

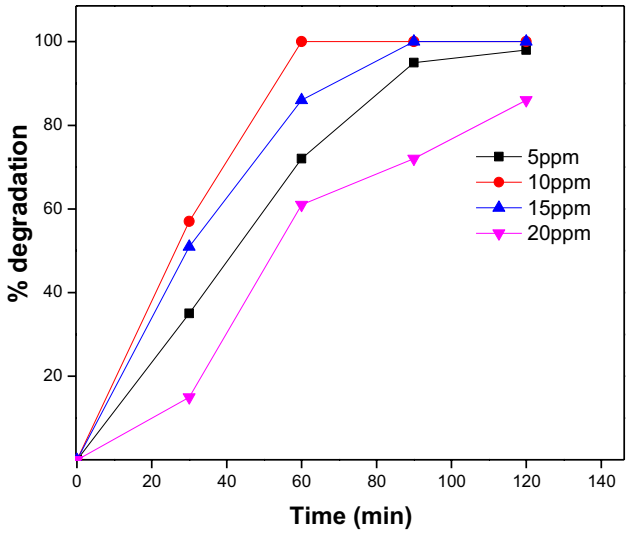

Fig. 11 Degradation of MB with varying concentration of dye and fixed weight of catalyst (10 mg)

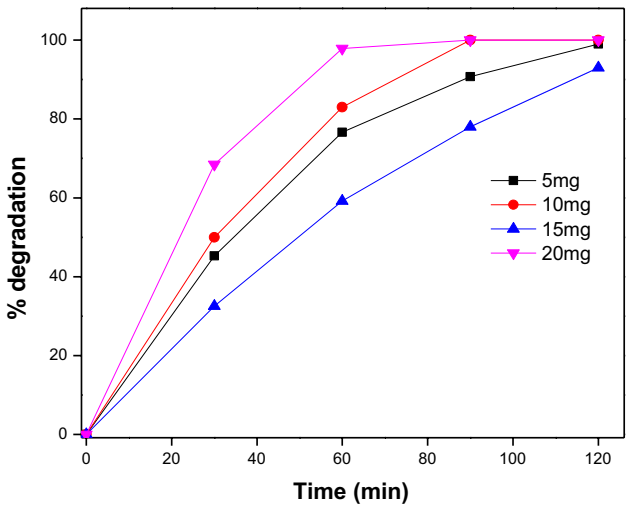

Fig. 12 Degradation of methylene blue with varying catalyst load and constant dye concentration

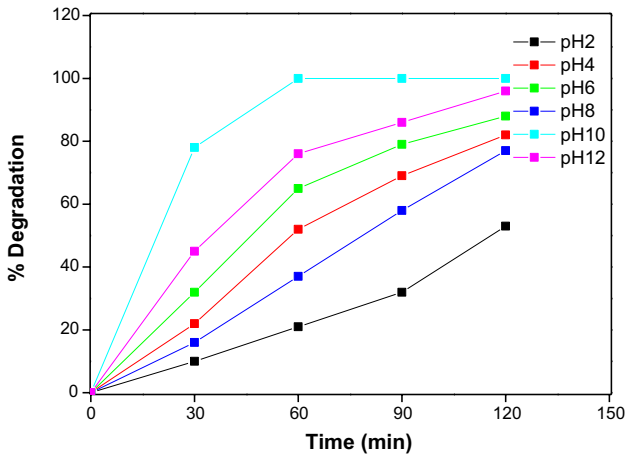

Fig. 13 Degradation of MB with varying pH of the solution and keeping the catalyst load and constant dye constant

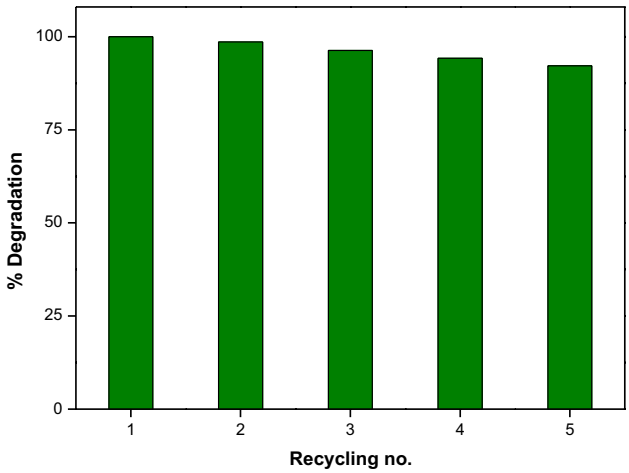

Fig. 14 Recycling of 10 mg of catalyst with 100 mL of 5 ppm dye

negatively charged surface. Due to the presence of many OH^- ions on the surface of catalyst, $OH^{\cdot}$ radical generation is lowered and which act as primary oxidizing agents and are responsible for lowering the degradation of MB dye [40–43].

4.4 Catalyst recycling

To evaluate the stability of the photocatalyst, a recycling experiment was carried out to degradation the methylene blue dye (Fig. 14). The experiment was done with catalyst (10 mg) and 5 ppm dye (100 mL). The stability of the catalyst checked by removing the catalyst by filtration, washed with ethanol and dried at 120 oC used for new cycles. Degradation of MB process was repeated for five cycles. In each cycle nearly 98–95% of MB were degraded with visible light irradiation which indicates that there is no loss of activity of catalyst [44]. The same experiment was also carried out with pure ZnO shows poor degradation of MB dye. The generation of excitons in pure ZnO was not easy due to the large bandgap and insufficient wavelength of visible light [45]. The efficiency of degradation of MB was almost the same for 5 cycles. It clearly shows the reduction of efficiency about nearly 8% for five cycles catalyst recycling.

4.5 Mechanism

Scheme A schematic representation of the degradation of MB using Ag–ZnO is shown below (Scheme 1).

$ZnO + h\nu \rightarrow ZnO\ (h^{+}_{vb} + e^{-}_{cb})$

$OH^{-}_{ads} + h^{+}_{vb} \rightarrow OH^{\cdot}_{ads}$ (in basic medium)

$MB + OH^{\cdot}_{ads} \rightarrow$ dye degradation

4.6 Detection of $OH^{\cdot}$ Radicals

$OH^{\cdot}$ (hydroxyl radical) is an unstable and reactive chemical species that is more important for the degradation of organic dyes using Coumarin as a probe molecule. This is a simple and sensitive method for OH radical detection. Coumarin reacts with OH radicals to form the 7-hydroxyl Coumarin, a luminous material that exhibits a PL peak at 456 nm.

In this process, 130 mg of ZnO was dispersed in 50 mL of 1 mM coumarin aqueous solution irradiated with UV light of 120 W. 2 mL of Aliquots of sample collected for every 10 min and the PL spectra was measured using Cary eclipse spectroflorimeter (Fig. 15). It shows that the formation of $OH^{\cdot}$ increases with an increase of time. This $OH^{\cdot}$ is responsible for the degradation of organic dyes [46].

5 Photoluminescence study

The PL study is a useful method for determining the efficiency of charge carrier separation in semiconductors [47]. Figure 16b shows the PL emission spectrum of ZnO and Ag–ZnO Nps taken at room temperature with an excitation wavelength of 380 nm. The pure ZnO nanoparticles

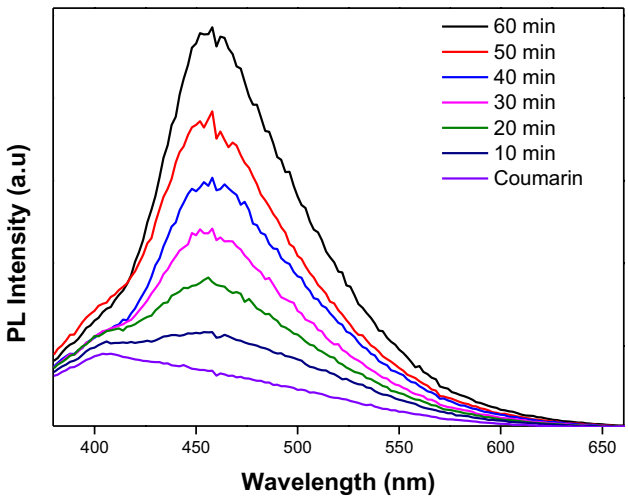

Fig. 15 PL spectrum of coumarin/hydroxyl coumarin under different time of irradiation

Scheme 1 Graphical representation for the degradation of MB with Ag–ZnO under the irradiation of UV light

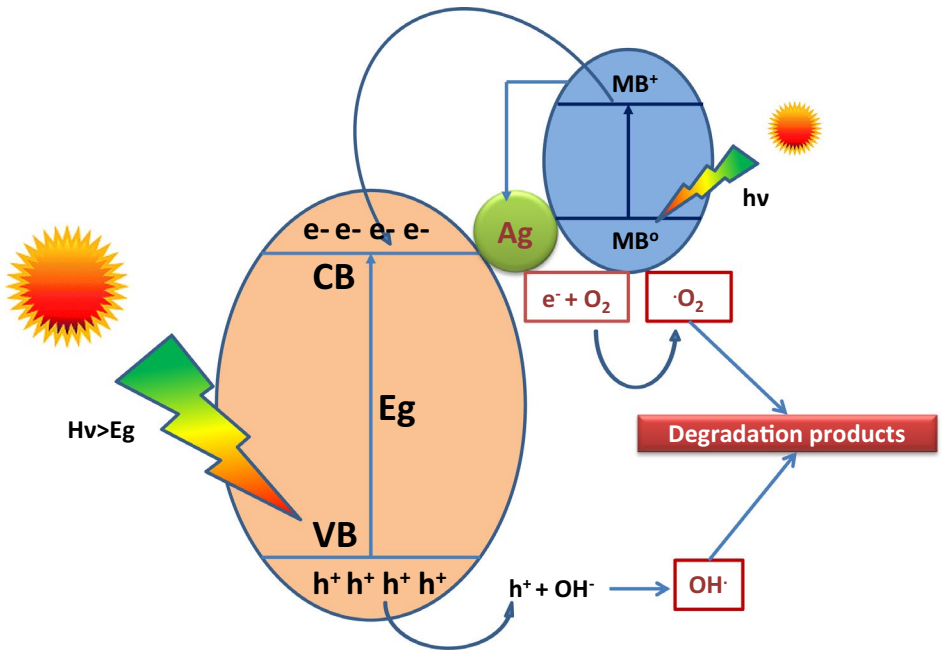

Mechanism.1. Graphical representation for the degradation of MB with Ag-ZnO under the irradiation of UV light

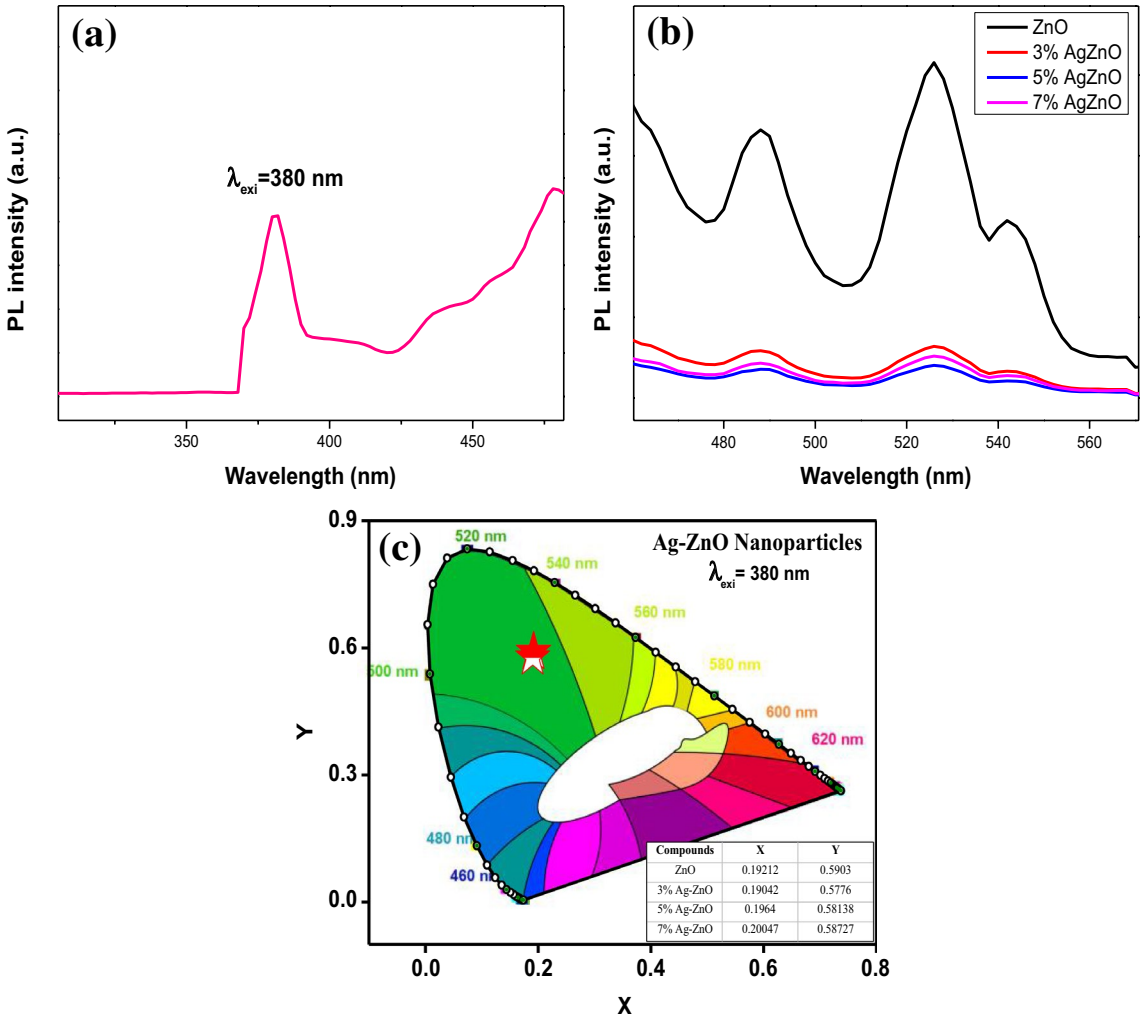

Fig. 16 PL spectrum of ZnO and Ag–ZnO **a** excitation spectra, **b** emission spectra, **c** CIE diagram

exhibit a strong UV emission peak at 525 nm and also a weak emission peak at 488 nm. In Ag–ZnO nanoparticles, there is a decrease of intensity in PL spectrum which is in acceptable criteria with the Stern–Volmer quenching process, this indicates a higher charge carrier separation efficiency for Ag–ZnO Nps. The emission peaks obtained are in UV and visible region and could be attributed to bound excitons and defect states located on the surface of nanostructured pure and doped ZnO Nps. Figure 16a shows a PL excitation spectrum with emission at 542 nm [48, 49].

The color coordinates are used to find out the emission color of the material. It can be estimated by the Commission's international De l'Eclairage system (CIE). Figure 16c represents the CIE diagram of ZnO and Ag–ZnO nanoparticles and it clearly reveals that both the materials are emitting the green colored light.

6 Conclusion

ZnO and Ag–ZnO Nps are successfully synthesized by solution combustion method using *Azadirachta indica* gum as a fuel. The NPs are confirmed by XRD and FTIR studies. The TEM analysis showed spherical shape with 15 nm particle size. Ag-doped ZnO acts as a good photocatalyst for the degradation of methylene blue due to the presence of Ag, which reduced the electron–hole recombination on the surface of the catalyst. Hence synthesized material is measured as a potent aspirant for the degradation of MB dye. In addition, it also shows the PL spectrum and it will be using for the green emitting LED applications.

Acknowledgements Mr. Udayabhanu gratefully acknowledge Council of Scientific and Industrial Research (CSIR), New Delhi for Senior Research Fellowship (SRF) (09/1204(0001)2018-EMR-I). Dr. GN thanks DST-Nanomission (SR/NM/NS-1262/2013) for financial support. Dr. GN also acknowledges Dr. Suresh Kumar H M, Department of Physics,

SIT, Tumakuru, for providing UV-DRS studies (VGST, Govt. of Karnataka). Mr. Basavalingiah thanks SIT for providing lab facilities.

Compliance with ethical standards

Conflict of interest The authors declare that they have no conflict of interest.

References

1. Lachheb H, Puzenat E, Houas A, Ksibi M (2002) Photocatalytic degradation of various types of dyes in water by UV-irradiated titania Appl Catal B: Environ 39:75–90
2. Gregorio C (2006) Non-conventional low-cost adsorbents to dye removal. A review. Bioresour Technol 97:1061–1085
3. Sreedhar S, Kotaiah B (2006) Comparative evaluation of commercial and sewage sludge based activated carbons for the removal of textile dyes from aqueous solutions. Iran J Environ Health Sci Eng 3:239–246
4. Bidhendi GN, Torabian A, Ehsani H, Razmkhah N (2007) Evaluation of industrial dyeing wastewater treatment with coagulants and polyelectrolyte as a coagulant aid. Iran J Environ Health Sci Eng 4:29–36
5. Espulgas SJ, Gimenez S, Contreras EP, Rodriguez M (2002) Comparison of different advanced oxidation processes for phenol degradation. Water Res 36:1034–1042
6. Rajan PI, Vijaya JJ, Jesudoss SK, Kaviyarasu K, Kennedy LJ, Jothiramalingam R, Al-Lohedan HA, Vaali-Mohammed MA (2017) Green-fuel-mediated synthesis of self-assembled NiO nanosticks for dual applications—photocatalytic activity on Rose Bengal dye and antimicrobial action on bacterial strains. Mater Res Express 4:085030
7. Ezhilarasi AA, Vijaya JJ, Kaviyarasu K, Kennedy LJ, Ramalingam RJ, Al-Lohedan HA (2018) Green synthesis of NiO nanoparticles using Aegle marmelos leaf extract for the evaluation of in-vitro cytotoxicity, antibacterial and photocatalytic properties. J Photochem Photobiol B: Biol 180:39–50
8. Anand K, Kaviyarasu K, Muniyasamy S, Roopan SM, Gengan RM, Chuturgoon AA (2017) Bio-synthesis of silver nanoparticles using agroforestry residue and their catalytic degradation for sustainable waste management. J Clust Sci 28:2279–2291
9. Parsons S (2004) Advanced oxidative processes for water and wastewater treatment. IWA Publishing, London
10. Chauhan R, Kumar AS, Chaudhary R (2011) Structure and optical properties of $Zn_{1-x}Ni_xO$ nanoparticles by coprecipitation method. J Optoelectron Biomed Mater 3:17–23
11. Bagheri S, Chandrappa KG, Hamid SA (2013) Facile synthesis of nano-sized ZnO by direct precipitation method. Der Pharma Chem 5:265–270
12. Seil JT, Webster TJ (2012) Antibacterial effect of zinc oxide nanoparticles combined with ultrasound. Nanotechnology 23:495101
13. Alivov YI, Kalinina EV, Cherenkov AE, Look DC, Ataev BM, Omaev AK, Bagnall DM (2003) Fabrication and characterization of n-ZnO/p-AlGaN heterojunction light-emitting diodes on 6H–SiC substrates. Appl Phys Lett 83:4719–4721
14. Dasa D, Chandra B, Phukonc NP, Kalitaa A, Doluia SK (2013) Surface area to volume ratios of ZnO NPs are responsible for significant higher antibacterial activities. Colloids Surf B: Biointerfaces 111:556–560
15. Calestani D, Zha M, Mosca R, Zappettini A, Carotta MC, Di Natale V, Zanotti L (2010) Growth of ZnO tetrapods for nanostructure-based gas sensors. Sens Actuat B: Chem 144:472–478
16. Li-Xia L, Qin-Xin T, Chang-Lu S, Yi-Chun L (2005) Structure and photoluminescence of nano-ZnO films grown on a Si (100) substrate by oxygen-and argon-plasma-assisted thermal evaporation of metallic Zn. Chin Phys Lett 22:998
17. Pillai SC, Kelly JM, Ramesh R, McCormack DE (2013) Advances in the synthesis of ZnO nanomaterials for varistor devices. J Mat Chem C 1:3268–3281
18. Wang ZL (2004) Zinc oxide nanostructures: growth, properties and applications. J Phys: Condens Matter 16:R829
19. Nagaraju G, Ashoka S, Chithaiah P, Tharamani CN, Chandrappa GT (2010) Surfactant free hydrothermally derived ZnO nanowires, nanorods, microrods and their characterization. Mater Sci Semicond Process 13:21–28
20. Ashoka S, Nagaraju G, Tharamani CN, Chandrappa GT (2009) Ethylene glycol assisted hydrothermal synthesis of flower like ZnO architectures. Mater Lett 63:873–876
21. Nagaraju G, Shivaraju GC, Banuprakash G, Dinesh R (2017) Photocatalytic activity of ZnO nanoparticles: synthesis via solution combustion method. Mater Today: Proc 4:11700–11705
22. Bhat S, Shrisha BV, Naika KG (2013) Synthesis of ZnO nanostructure by solvothermal method. Arch Phy Res 4:61–70
23. Moazzen M, Borghei SM, Taleshi F (2012) Synthesis and characterization of nano-sized hexagonal and spherical nanoparticles of zinc oxide. J Nano Sci 2:295–300
24. Mukherjee S, Srivastava HC (1955) The structure of neem gum. J Am Chem Soc 77:422–423
25. Phattepur H, Siddaiah GB, Ganganagappa N (2019) Synthesis and characterisation of mesoporous TiO_2 nanoparticles by novel surfactant assisted sol-gel method for the degradation of organic compounds. Periodica Polytech Chem Eng 63:85–95
26. Wang T, Jiao Z, Chen T, Li Y, Ren W, Lin S, Lu G, Ye J, Bi Y (2013) Vertically aligned ZnO nanowire arrays tip-grafted with silver nanoparticles for photoelectrochemical applications. Nanoscale 5:7552–7557
27. Zamiri R, Rebelo A, Zamiri G, Adnani A, Kuashal A, Belsleyd MS, Ferreira JMF (2014) Far-infrared optical constants of ZnO and ZnO/Ag nanostructures. RSC Adv 4:20902–20908
28. Hower P, Gupta T (1979) A barrier model for ZnO varistors. J Appl Phys 50:4847–4855
29. Wahab R, Ansari SG, Kim YS, Seo HK, Kim GS, Khang G, Shin HS (2007) Low temperature solution synthesis and characterization of ZnO nano-flowers. Mater Res Bull 42:1640–1648
30. Udayabhanu Nagaraju G, Nagabhushana H, Basavaraj RB, Raghu GK, Suresh D, Rajanaika H, Sharma SC (2016) Green, nonchemical route for the synthesis of ZnO superstructures, evaluation of its applications toward photocatalysis, photoluminescence and biosensing. Cryst Growth Des 16:6828–6840
31. Ezhilarasi AA, Vijaya JJ, Kaviyarasu K, Maaza M, Ayeshamariam A, Kennedy LJ (2016) Green synthesis of NiO nanoparticles using Moringa oleifera extract and their biomedical applications: cytotoxicity effect of nanoparticles against HT-29 cancer cells. J Photochem Photobiol B: Biol 164:352–360
32. Vijaya JJ, Jayaprakash N, Kombaiah K, Kaviyarasu K, Kennedy LJ, Ramalingam RJ, Al-Lohedan HA, Mansoor-Ali VM, Maaza M (2017) Bioreduction potentials of dried root of Zingiber officinale for a simple green synthesis of silver nanoparticles: antibacterial studies. J Photochem Photobiol B: Biol 177:62–68
33. Saravanakkumar D, Sivaranjani S, Kaviyarasu K, Ayeshamariam A, Ravikumar B, Pandiarajan S, Veeralakshmi C, Jayachandran M, Maaza M (2018) Synthesis and characterization of ZnO–CuO nanocomposites powder by modified perfume spray pyrolysis method and its antimicrobial investigation. J Semicond 39:033001

34. Suresh D, Nethravathi PC, Udayabhanu Rajanaika H, Nagabhushana H, Sharma SC (2015) Green synthesis of multifunctional zinc oxide (ZnO) nanoparticles using Cassia fistula plant extract and their photodegradative, antioxidant and antibacterial activities. Mater Sci Semicond Process 31:446–454
35. Zheng Y, Chen C, Zhan Y, Lin X, Zheng Q, Wei K, Zhu J (2008) Photocatalytic activity of Ag/ZnO heterostructure nanocatalyst: correlation between structure and property. J Phys Chem C 112:10773–10777
36. Suresh D, Nethravathi PC, Lingaraju K, Rajanaika H, Sharma SC, Nagabhushana H (2015) EGCG assisted green synthesis of ZnO nanopowders: photodegradative, antimicrobial and antioxidant activities. Spectrochim Acta Part A: Mol Biomol Spectrosc 136:1467–1474
37. Madan HR, Sharma SC, Suresh D, Vidya YS, Nagabhushana H, Rajanaik H, Anantharaju KS, Prashantha SC, Maiya PS (2016) Facile green fabrication of nanostructure ZnO plates, bullets, flower, prismatic tip, closed pine cone: their antibacterial, antioxidant, photoluminescent and photocatalytic properties. Spectrochim Acta Part A: Mol Biomol Spectrosc 152:404–416
38. Khodja AA, Sehili T, Pilichowski JF, Boule P (2001) Photocatalytic degradation of 2-phenylphenol on TiO_2 and ZnO in aqueous suspensions. J Photochem Photobiol A: Chem 141:231–239
39. Anandan S, Vinu A, Lovely KS, Gokulakrishnan N, Srinivasu P, Mori T, Murugesan V, Sivamurugan V, Ariga K (2007) Photocatalytic activity of La-doped ZnO for the degradation of monocrotophos in aqueous suspension. J Mol Catal A: Chem 266:149–157
40. Poulios I, Tsachpinis I (1999) Photodegradation of the textile dye Reactive Black 5 in the presence of semiconducting oxides. J Chem Technol Biotechnol: Int Res Process Environ Clean Technol 74:349–357
41. Liqiang J, Xiaojun S, Baifu X, Baiqi W, Weimin C, Honggang F (2004) The preparation and characterization of La doped TiO_2 nanoparticles and their photocatalytic activity. J Solid State Chem 177:3375–3382
42. Mills A, Davies RH, Worsley D (1993) Water purification by semiconductor photocatalysis. Chem Soc Rev 22:417
43. Rengaraj S, Li XZ (2006) Photocatalytic degradation of bisphenol A as an endocrine disruptor in aqueous suspension using Ag–TiO_2 catalysts. Int J Environ Pollut 27:20
44. Reddy YS, Magdalane CM, Kaviyarasu K, Mola GT, Kennedy J, Maaza M (2018) Equilibrium and kinetic studies of the adsorption of acid blue 9 and Safranin O from aqueous solutions by MgO decked FLG coated Fuller's earth. J Phys Chem Solids 123:43–51
45. Magdalane CM, Kaviyarasu K, Raja A, Arularasu MV, Mola GT, Isaev AB, Al-Dhabi NA, Arasu MV, Jeyaraj B, Kennedy J, Maaza M (2018) Photocatalytic decomposition effect of erbium doped cerium oxide nanostructures driven by visible light irradiation: investigation of cytotoxicity, antibacterial growth inhibition using catalyst. J Photochem Photobiol B: Biol 185:275–282
46. Vinay SP, Nagarju G, Chandrappa CP, Chandrasekhar N (2019) Enhanced photocatalysis, photoluminescence, and anti-bacterial activities of nanosize Ag: green synthesized via *Rauvolfia tetraphylla* (devil pepper). SN Appl Sci 1:477
47. Nagaraju G, Nagabhushana H, Suresh D, Anupama C, Raghu GK, Sharma SC (2017) Vitis labruska skin extract assisted green synthesis of ZnO super structures for multifunctional applications. Ceram Int 43:11656–11667
48. Nagaraju G, Prashanth SA, Shastri M, Yathish KV, Anupama C, Rangappa D (2017) Electrochemical heavy metal detection, photocatalytic, photoluminescence, biodiesel production and antibacterial activities of Ag–ZnO nanomaterial. Mater Res Bull 94:54–63
49. Basavalingiah KR, Udayabhanu, Harishkumar S, Nagaraju G, Chikkahanumantharayappa, (2019) NiO and Ag@NiO nanomaterials for enhanced photocatalytic and photoluminescence studies: green synthesis using *lycopodium linn*. Asian J Eng Appl Technol 8:79–85